Soft Matter

PAPER

Cite this: *Soft Matter*, 2019, **15**, 1869

Evolution of ligand-capped nanoparticle multilayers toward a near unique thickness†

Mala Mukhopadhyay ‡ and S. Hazra *

The structural evolution of thiol-capped Au-nanoparticle (AuNP) multilayers on a H-passivated Si substrate, formed through a Langmuir–Schaefer (LS) deposition process, has been investigated using complementary grazing incidence X-ray scattering techniques. The fractional coverage multilayers of AuNPs, formed through a multi-transfer process, are found to be quite unstable under ambient conditions. The thickness of these decreases with time and tends to saturate toward a near unique thickness (NUT $\approx$ 6 nm). Although initial low coverage and their instability create hindrance in the control and formation of desired 3D-nanostructures in the bottom-up approach, the formation of a NUT-layer, through time-evolution, is quite distinctive, thus interesting. It is clear from the evolution that the thermodynamically driven monolayer structures (of AuNPs) at the air–water interface become thermodynamically unstable when transferred sequentially onto the solid substrate. The thermal energy (kT) and the partial change in the substrate surface energy ($\Delta\gamma$) create the instability and induce diffusion in the AuNPs, which in the presence of a net attractive force towards the substrate (arising from anisotropic interaction of the top AuNPs with the other AuNPs and/or hydrophobic substrate) tries to create a thermodynamically favourable and relatively stable NUT-layer through reorganization for a different duration. This happens if the number of AuNPs is less than or equal to the maximum number that can be accommodated within the NUT. The value of the NUT mainly depends on the particle size and a kT-energy related fluctuation of particles. Furthermore, the formation of the NUT-layer indicates that the hydrophobic–hydrophobic interaction mediated net attraction towards the substrate is long range, while the hydrophilic–hydrophobic interaction mediated repulsion and/or kT-energy induced fluctuations are short range.

Received 4th December 2018,
Accepted 22nd January 2019

DOI: 10.1039/c8sm02449a

rsc.li/soft-matter-journal

1 Introduction

Metal nanoparticles (NPs), which are most often stabilized with organic ligands, show distinctive properties that are unseen in their larger counterparts or in bulk.[1,2] The hard metallic core is mainly responsible for producing distinctive properties, while the soft ligand shell provides a buffer between NPs even without the presence of solvent.[3,4] The self-assembly of such NPs can form two and three dimensional (2D and 3D) structures, which are promising candidates for many applications related to optical, magnetic, electrical and catalytic properties, stemming from the collective features of the ordered NPs.[5–14] Understanding such ordering is one of the prerequisites for possible applications of the self-assembled nanostructures.

Thiol-capped gold NPs (AuNPs), due to their ease of preparation following the Brust method and their ability to form large arrays through spontaneous self-assembly, constitute one such nanostructure system, which has been studied extensively.[15–24] It is known from these studies that, at the air/water interface, AuNPs self-assemble to form 2D-structures, which then can be transferred onto a solid substrate using Langmuir–Blodgett (LB) and Langmuir–Schaefer (LS) deposition techniques to grow 2D- and 3D-nanostructures over large areas.[17,19,22–24] Among these structures, the nanostructures grown on hydrophobic substrates using the LS technique are of special interest,[22,24] as the interaction between the hydrophobic AuNP-shell and a hydrophobic substrate (*i.e.* between two hydrophobic or similar nature materials) is attractive. This is likely to create the least disturbance on the structure during transfer and thus is expected to be better controlled. Although some work has been carried out to understand the structure and growth of LS monolayers of AuNPs on hydrophobic substrates (*i.e.* 2D-nanostructures),[24] no work has been carried out to understand the growth and stability of LS multilayers of AuNPs on hydrophobic substrates, which is of utmost importance for the formation of desired 3D-nanostructures of specific collective properties through a controlled bottom-up technique.

Saha Institute of Nuclear Physics, 1/AF Bidhannagar, Kolkata 700064, India. E-mail: satyajit.hazra@saha.ac.in

† Electronic supplementary information (ESI) available. See DOI: 10.1039/c8sm02449a

‡ Current address: BRA Bihar University, Muzaffarpur 842001, India.

The study of LS monolayers of AuNPs on hydrophobic substrates, on the other hand, suggests that apart from the hydrophobic nature of the substrate, the hydrophobic strength is responsible for creating minimum disturbance on the Langmuir monolayers.[24] In fact, it was found that the weak-hydrophobic H-passivated Si substrate creates less disturbance, compared to the strong-hydrophobic OTS self-assembled Si substrate, to better mimic the Langmuir monolayer structures. Such structures were again found to evolve with time under ambient conditions (due to the presence of room temperature thermal energy and/or the change in interfacial energy) to form similar vertically expanded monolayer structures. The conditions for obtaining the better mimic structure at the initial stages and the formation of similar vertically expanded monolayer structures through evolution for LS monolayers are interesting, and lead to the questions: (i) can the desired 3D-structures be formed on a H-passivated Si substrate through the multi-transfer of such Langmuir monolayers, at least at the initial stages, simply by knowing and controlling the Langmuir monolayer structures, *i.e.* is the mimic concept valid for the multi-transferred LS films? (ii) Do the multi-transferred LS films evolve into similar vertically expanded monolayer structures, *i.e.* can the evolution of multilayer LS films infer anything about the uniqueness in the thickness of the evolved structure and its possible origin? It can be noted that keeping the LS film for a long time may cause some structural changes (toward an energy minimum state) as the transfer process itself is not always carried out under equilibrium conditions. Hence, finding the energy minimum state or structure and the associated processes are quite in demand, although challenging.

In this paper we have addressed these questions by investigating the structures of the multi-transferred LS films of AuNPs on H-Si substrates using complementary X-ray reflectivity (XR)[25–29] and grazing incidence small angle scattering (GISAXS) techniques,[22,30,31] and their evolution with time under ambient conditions using an XR technique.[24,32,33] It is found that the structures of the films, at the initial stages, depend strongly on the surface pressure of the Langmuir monolayer and the number of transfers but follow weakly the Langmuir monolayer structure, both in terms of layer coverage and domain structure. On the other hand, it is indeed found that the structure (thickness) of the film evolves (decreases) with time under ambient conditions approaching towards a near unique thickness (provided that the amount of transferred AuNPs in the LS film is within the amount which can be accommodated). The possible interactions and/or energy, responsible for the growth of such near unique thickness from different layer-number and layer-coverage films, through evolution, are discussed.

2 Experimental section

2.1 Preparation of *m*T-AuNP/H-Si LS films

The colloidal AuNPs with a core (Au) size of about 2.5 ± 0.6 nm and an overall (Au plus thiol shell) size of about 4.5 ± 0.6 nm were synthesized following a two-phase (water–toluene) reduction of hydrogen tetrachloroaurate by sodium borohydride in the presence of dodecanethiol,[15,34] as previously reported (also presented in the ESI†).[22] These AuNPs were spread uniformly on the surface of water (Milli-Q) in a Langmuir trough (KSV 5000) to form a Langmuir monolayer.[22] The pressure (Π) of the AuNP Langmuir monolayer was regulated by movement of the Teflon barriers. Prior to the AuNP Langmuir monolayers transfer, Si substrates (of a size about 15 × 15 mm^2) were first sonicated in organic solvents to remove organic contaminates and then treated with a hydrogen fluoride solution [HF, Merck, 10%] to prepare H-terminated Si (H-Si) substrates.[22,35] The AuNP Langmuir monolayers formed at different pressures (namely Π = 2, 4, 6, 10 and 14 mN m^{-1}) were then transferred twice (2T) and four times (4T) onto the H-Si substrates using the LS deposition technique (as detailed in the ESI†).[22,36] Such multi-transferred films are labeled as *m*T-AuNP/H-Si LS films, where m = 2 and 4. The films were then preserved at the X-ray laboratory, where the temperature and relative humidity were maintained at ~25 °C and ~40%, respectively.

2.2 Characterization of *m*T-AuNP/H-Si LS films

The characterization of *m*T-AuNP/H-Si LS films, within a day, after a month and after a year of preparation, were carried out using the XR technique, while characterization at the initial stages was also carried out using a complementary GISAXS technique. In the scattering measurements, the sample surface was in the x–y plane and the incident X-ray beam (of wavelength λ) was in the x–z plane. α is the incident angle with the x–y plane, β is the exit angle with the x–y plane and ϕ is the exit angle with the x–z plane.

XR measurements of the films were performed on a versatile X-ray diffractometer (VXRD) setup.[22,27,37] VXRD consists of a diffractometer (D8 Discover, Bruker AXS) with a Cu source (sealed tube) followed by a Göbel mirror to select and enhance Cu Kα radiation (λ = 1.54 Å). The diffractometer has a two-circle goniometer [$\theta(\omega)$–2θ] with a quarter-circle Eulerian cradle as a sample stage. The latter has two circular (χ and ϕ) and three translational (X, Y, and Z) motions. The scattered beam was detected using a NaI scintillation (point) detector. Data were taken under specular conditions, *i.e.* for φ = 0 and $\alpha = \beta = \theta$. Under such conditions there exists a nonvanishing wave vector component, q_z, which is equal to $(4\pi/\lambda)\sin\theta$ with a resolution of 0.002 $Å^{-1}$. The XR technique essentially provides an electron-density profile (EDP), *i.e.*, the in-plane (x–y) average electron density (ρ) as a function of depth (z) in high resolution.[32] From EDP it is possible to verify the presence of layering in the film, with their number, position and coverage.

GISAXS measurements of the films were carried out using a synchrotron source (MiNaXS beam line, PETRA III)[22,38–42] at λ = 0.94 Å. The scattered beam in the q_y–q_z plane was detected using a 2D detector (PILATUS 300k, Dectris, having 619 × 487 pixels with a pixel size of 172 × 172 μm^2), where $q_y = (2\pi/\lambda)\cos\beta\sin\phi$ and $q_z = (2\pi/\lambda)(\sin\beta + \sin\alpha)$. To avoid saturation of the detector, the direct beam was stopped and the specular reflected beam was attenuated by two separate point-like beam stops. The sample-to-detector distance was 1721 mm. The corresponding angular

resolution was 0.1 mrad and the resolution limit along the q_y-direction was less than 0.002 Å^{-1}.[22] For data collection, the incident angle α was kept at 0.25°, slightly greater than the critical angle, α_c, of the sample. The GISAXS pattern on a particular position was collected for a small amount of time (10 s) to minimize the effect of radiation damage of the sample. Then GISAXS patterns were collected at different lateral positions of a sample to rule out the in-plane inhomogeneity of the sample and to enhance the statistics by averaging.

3 Results and discussion

3.1 XR studies of the as-grown films

The XR data of the *m*T-AuNP/H-Si LS films deposited at different Π-values and collected within a day (*i.e.* $t < 1$ day) are shown in Fig. 1. Oscillations with more than a single periodicity are observed in all the XR profiles. The high frequency oscillations are the Kiessig fringes corresponding to the total film thickness. The relatively strong peaks near $q_z \approx 0.18$ and 0.37 Å^{-1} (indicated by dashed lines) are the first and second order pseudo-Bragg peaks corresponding to the layered structures of the films, the position and intensity of which change slightly with the Π-value and also with the *m*-value.

To get quantitative information about the films, all the XR profiles were analyzed using Parratt's formalism,[43] after incorporating roughness at each interface.[22,32] Instrumental resolution in the form of a Gaussian function and a constant background were also included at the time of data analysis. For the analysis, 2T- and 4T-AuNP/H-Si LS films were first modelled with two and four layers, respectively, of AuNPs of different thickness and coverage on the Si substrates. Where each AuNP layer consists of three layers, namely a thiol-rich low density bottom layer, an Au-rich high density middle layer and again a thiol-rich low density top layer. Hence, the 2T- and 4T-AuNP/H-Si LS films were actually analysed using 5 and 9 layers, respectively, of alternate low and high electron densities. The best fit XR profiles along with the corresponding EDPs for the *m*T-AuNP/H-Si LS films are shown in Fig. 1.

Two and four peaks are readily evident in the EDPs (insets of Fig. 1) of the 2T- and 4T-AuNP/H-Si LS films, suggesting bilayer and tetralayer natures, respectively. However, the peak value (ρ_m) is not the same for the different peak positions in a film and also for the similar peak position in different films. The variation of such ρ_m-values for different layer numbers (n) in the *m*T-AuNP/H-Si LS films are plotted in Fig. 2 as a function of the Π-value. In the case of the 2T-AuNP/H-Si LS films, the ρ_m-value for the first layer was found to be relatively high, which increased quickly initially then slowly (*i.e.* exponentially) with the Π-value, while that of the second layer was relatively low and decreased exponentially with the Π-value. In the case of the 4T-AuNP/H-Si LS films, however, the ρ_m-value for the first and second layers decreased gradually with the Π-value, except for a high Π-value, while that for the third and forth layers increased gradually with the Π-value.

The variation of the ρ_m-value and the peak position (z_m) with layer number are also plotted in Fig. 2 for the *m*T-AuNP/H-Si LS films deposited at two extreme Π-values (namely 2 and 14 mN m^{-1}). The average out-of-plane separation between the layers (d_{out}) obtained from the slope of the z_m *vs.* n curves for the four films are tabulated in Table 1. The d_{out}-value (~3.1 nm) was quite small compared to the overall size of the AuNPs ($2R \approx 4.5$ nm)

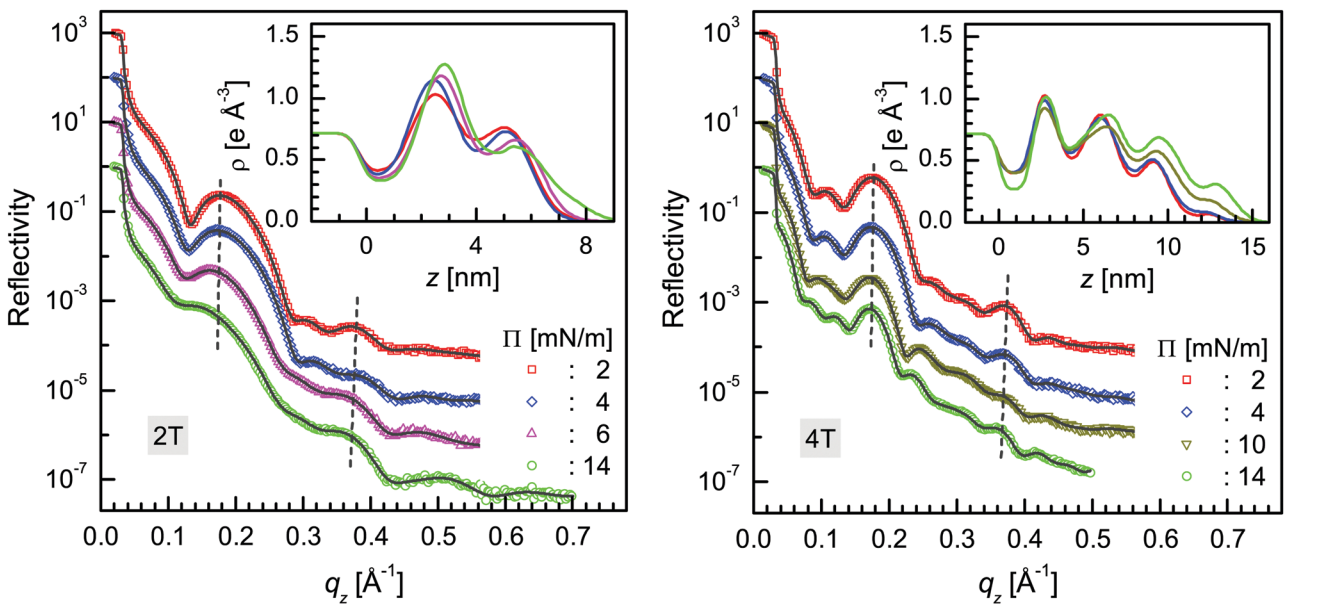

Fig. 1 X-ray reflectivity data (different symbols) collected within a day ($t < 1$ day) and the analysed curves (solid lines) of multi-transferred (2T- and 4T-) AuNP/H-Si LS films prepared from the Langmuir monolayers of different surface pressures (Π). Curves are shifted vertically for clarity. First order and second order psudo-Bragg peaks arising from out-of-plane AuNP layer separation (d_{out}) are indicated by dashed lines. Insets: corresponding analysed electron density profiles.

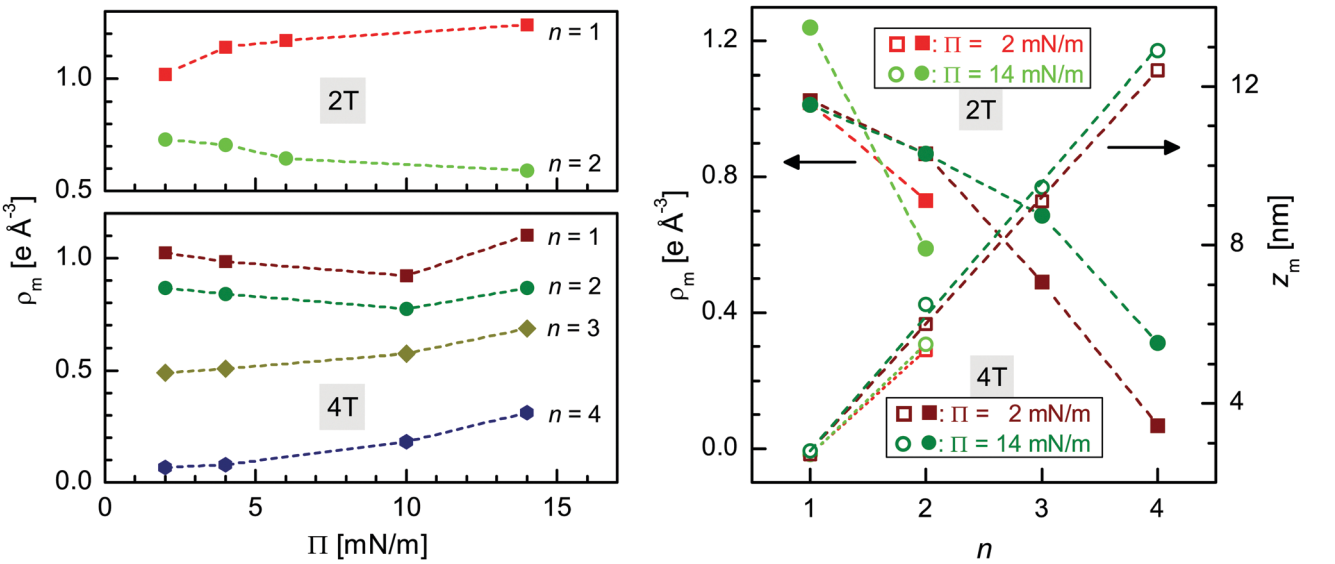

Fig. 2 Left: variation of the peak electron density (ρ_m) with deposited surface pressure (Π) for the different layer numbers (n) in the EDPs of multi-transferred (2T- and 4T-) AuNP/H-Si LS films. Right: variation of the peak electron density (ρ_m) and peak position (z_m) with the layer number (n) in the EDPs of multi-transferred (2T- and 4T-) AuNP/H-Si LS films prepared from the Langmuir monolayers of two different surface pressures (Π).

Table 1 Parameters such as the in-plane AuNPs separation (d_{in}) and out-of-plane AuNP layers separation (d_{out}) at the initial stages; the total film thickness (D) and the average electron density (ρ_{ave}) at the different ageing times (t) for the multi-transferred mT-AuNP/H-Si LS films deposited at different surface pressures (Π), as obtained from the GISAXS and XR data analysis

		t < 1 day				$t \approx$ 1 month		$t \approx$ 1 year	
mT	Π [mN m^{-1}]	d_{in} [nm]	d_{out} [nm]	D [nm]	ρ_{ave} [e Å^{-3}]	D [nm]	ρ_{ave} [e Å^{-3}]	D [nm]	ρ_{ave} [e Å^{-3}]
2T	2	3.9	2.8	6.4 ± 0.6	0.73	4.8 ± 1.0	0.97	4.6 ± 0.9	1.02
	14	4.6	2.9	6.8 ± 0.6	0.73	5.0 ± 1.2	0.99	4.5 ± 0.8	1.10
4T	2	4.0	3.2	13.1 ± 0.7	0.49	11.0 ± 1.7	0.59	6.2 ± 1.2	1.03
	14	4.2	3.4	13.9 ± 0.7	0.58	11.0 ± 1.5	0.70	7.1 ± 1.5	1.08

and was found to increase with the Π-value and also with the m-value. The average film thickness (D) and the average electron density (ρ_{ave}) obtained from the EDPs are also listed in Table 1. For the 2T-AuNP/H-Si LS films, the ρ_{ave}-value was found to be unchanged, while the D-value was found to increase slightly with the Π-value, suggesting a very small increase in the amount of transferred material. On the other hand, for the 4T-AuNP/H-Si LS films, both (ρ_{ave} and D) values were found to increase with the Π-value, suggesting a reasonable increase in the amount of transferred material. Furthermore, the ρ_{ave}-value was found to decrease considerably with the increase of the m-value from 2 to 4, suggesting a considerable decrease in the amount of material per transfer with the increase in the number of transfers.

3.2 GISAXS studies of the as-grown films

The GISAXS patterns of the mT-AuNP/H-Si LS films deposited at two extreme Π-values (2 and 14 mN m^{-1}) are shown in Fig. 3. Bragg rods around q_y = ±0.15 Å^{-1} are observed in all the patterns, the intensity and actual position of which varies with Π and m values. To have a better idea about the position and intensity of the Bragg rods, GISAXS line profiles along the q_y direction and through the Bragg rods, for all the films, are also plotted in Fig. 3. The line profiles along the q_y-direction clearly show peaks around q_y = ±0.15 Å^{-1} due to in-plane AuNP separation (d_{in}). The d_{in}-values obtained from the peak positions are tabulated in Table 1 for the four films. The d_{in}-value (~4.2 nm) is slightly low compared to the 2R-value but considerably high compared to the d_{out}-value. The d_{in}-value is also found to increase with the Π-value. The increase is, however, small for the 4T-AuNP/H-Si LS films but appreciable for the 2T-AuNP/H-Si LS films. The peak intensity for the 2T-AuNP/H-Si LS films decreases slightly with the increase of the Π-value, while for the 4T-AuNP/H-Si LS films it increases slightly with the increase of the Π-value. Further, to have a better idea about the different in-plane correlation lengths (especially the larger correlation lengths, which should appear at low q_y values), the log–log plot of the same GISAXS line profiles are presented in the insets of Fig. 3. A broad hump was observed for the 2T-AuNP/H-Si LS films (shown by the dashed lines), suggesting formation of domain-like structures in these films. The average separations between the domains, as obtained from the hump positions, are about 100 and 50 nm for the films with Π-values of 2 and 14 mN m^{-1}, respectively. This indicates that the separation between the domains decreases with the Π-value, which is probably due to the increase in the number of domains.

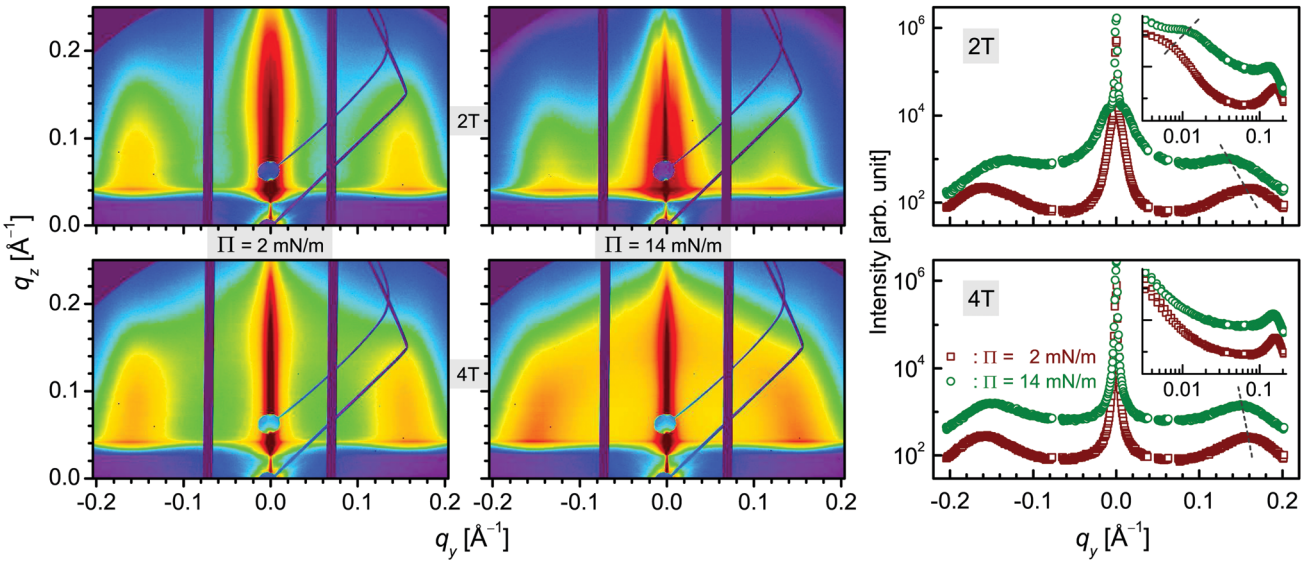

Fig. 3 Left panel: GISAXS patterns of multi-transferred (2T- and 4T-) AuNP/H-Si LS films prepared from the Langmuir monolayers of two extreme surface pressures (Π). Right panel: corresponding GISAXS line profiles along the q_y direction (*i.e.* lateral cut through the first Bragg rod at $q_z \approx 0.04$ Å^{-1}). Peaks arising from in-plane AuNPs separation (d_{in}) are indicated by dashed lines. Insets: log–log plot of the same GISAXS line profiles to have a better idea about the in-plane correlation at different length scales. Broad humps arising from an in-plane correlation between domain-like structures are indicated by dashed lines. Curves are shifted vertically for clarity.

The information about the domains for the 4T-AuNP/H-Si LS films is however missing.

3.3 XR studies of the films after a month

XR data of the *m*T-AuNP/H-Si LS films deposited at different Π-values and collected after a month (*i.e.* $t \approx 1$ month) are shown in Fig. 4. Oscillations with more than a single periodicity are observed in all the XR profiles. However, for the 2T-AuNP/H-Si LS films, the oscillations are very weak compared to the as-grown films and even the first order pseudo-Bragg peak is absent, which indicates the absence of a multi-layered structure. For the 4T-AuNP/H-Si LS films, although the first order pseudo-Bragg peak is present, it becomes broad and shifts toward a lower q_z value, which suggests a decrease in the layer number and an increase in the layer width. To get quantitative information of the 2T- and 4T-AuNP/H-Si LS films, the XR data were

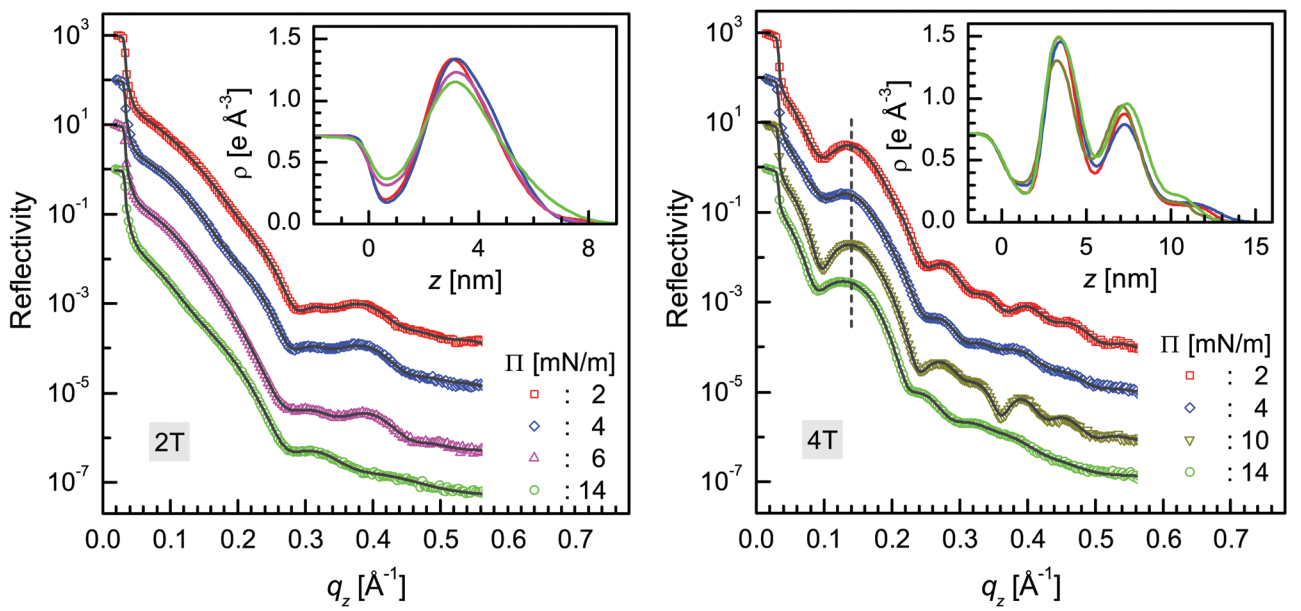

Fig. 4 X-ray reflectivity data collected after a month (different symbols) and analysed curves (solid lines) of multi-transferred (2T- and 4T-) AuNP/H-Si LS films prepared from the Langmuir monolayers of different surface pressures (Π). Curves are shifted vertically for clarity. Pseudo-Bragg peaks due to layered structures of the films are indicated by dashed lines. Insets: corresponding analysed electron density profiles.

analyzed using 3 and 7 layers, respectively, of alternate low and high electron densities.

The best fit XR profiles along with the corresponding EDPs for the *m*T-AuNP/H-Si LS films are shown in Fig. 4. Only one and two (with weak third) peaks are observed in the EDPs (the insets of Fig. 4) suggesting monolayer and bilayer (with some trilayer) natures of the 2T- and 4T-AuNP/H-Si LS films, respectively, after a month, deviating from the original bilayer and tetralayer natures. The *D*-values and the ρ_{ave}-values obtained from the EDPs for the four films are also listed in Table 1. For the 2T-AuNP/H-Si LS films, the *D*-value ($\sim$5 nm) was found to decrease $\sim$25%, and correspondingly the ρ_{ave}-value ($\sim$1 e Å^{-3}) was found to increase $\sim$30% compared to the values of the as-grown structures. On the other hand, for the 4T-AuNP/H-Si LS films, the *D*-value became about 11 nm for both the films, while the ρ_{ave}-value became about 0.6 and 0.7 e Å^{-3} for the films of Π = 2 and 14 mN m^{-1}, respectively, suggesting $\sim$20% decrease in the *D*-value and $\sim$20% increase in the ρ_{ave}-value of the films after a month.

3.4 XR studies of the films after a year

XR data of the *m*T-AuNP/H-Si LS films deposited at different Π-values and collected after a year (*i.e.* $t \approx 1$ year) are shown in Fig. 5. Weak oscillations are observed in all the XR profiles but the pseudo-Bragg peak is absent, indicating disappearance of the multi-layered structures of the films. The best fit XR profiles along with the corresponding EDPs for the *m*T-AuNP/H-Si LS films are also shown in Fig. 5. A single peak is observed in the EDPs (the insets of Fig. 5) suggesting the monolayer nature of the films, after a year, deviating from the original bilayer and tetralayer natures. The *D*-value and the ρ_{ave}-value obtained from the EDPs for the four films are listed in Table 1. For the 2T-AuNP/H-Si LS films, the *D*-value ($\sim$4.5 nm) is found to be appreciably low ($\sim$30%) compared to the value of the as-grown films, but slightly low compared to the value of the films observed after a month. Correspondingly the ρ_{ave}-value increases significantly ($\sim$35%) compared to the value of the as-grown films but increases negligibly compared to the value of the films observed after a month. On the other hand, for the 4T-AuNP/H-Si LS films, the *D*-value ($\sim$6.5 nm) was appreciably low ($\sim$50% and $\sim$40%), while the ρ_{ave}-value ($\sim$1.05 e Å^{-3}) was significantly high ($\sim$95% and $\sim$60%) compared to the values of the as-grown films and the films observed after a month.

3.5 Growth and stability of *m*T-AuNP/H-Si LS films

Let us now try to visualize the structures of the *m*T-AuNP/H-Si LS films at different stages (or times) and then discuss their growth and stability/instability. The visualization of the structures is possible through proper reconstructions or deconvolutions of the analysed EDPs. Now, taking into consideration (from the ESI†) that the EDP of a monolayer of AuNPs can be approximated by a simple Gaussian function, the analysed EDP can be deconvoluted using the following equation:

$$\rho(z) = \frac{\rho_s}{2}\left[1 - \mathrm{erf}\left(\frac{z - z_0}{\sigma_s}\right)\right] + \sum_i \rho_i \exp\left[-\left(\frac{z - z_i}{\sigma}\right)^2\right] \quad (1)$$

where the first term is an error function corresponding to the substrate of uniform electron density ρ_s with substrate surface (or film–substrate interface) roughness σ_s at position z_0, while the second term is the summation of Gaussian peaks of different intensities (ρ_i) and positions (z_i) but of the same standard deviation (σ, related to the peak-width). This second term is related to the film, which consists of a number of AuNP layers of similar thickness (represented by σ) but different coverage (represented by ρ_i) placed at different vertical positions (z_i).

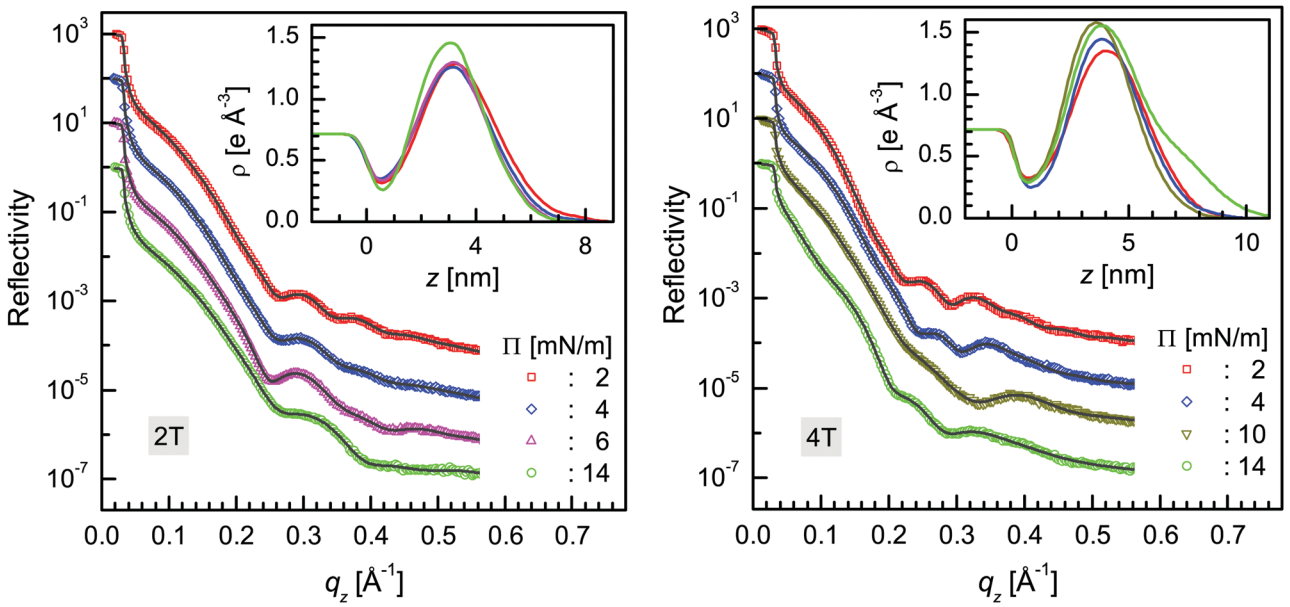

Fig. 5 X-ray reflectivity data collected after a year (different symbols) and analysed curves (solid lines) of multi-transferred (2T- and 4T-) AuNP/H-Si LS films prepared from the Langmuir monolayers of different surface pressures (Π). Curves are shifted vertically for clarity. Insets: corresponding analysed electron density profiles.

Eqn (1) was used to simulate the analysed EPDs. For the simulation, attempts were made to minimize the number of Gaussian peaks by optimizing the σ value. It was observed that σ = 1.15 nm, which corresponds to the near monolayer structure (as evident from the ESI†), can well simulate the analyzed EDPs. Deconvoluted profiles obtained from the simulation of the analysed EDPs for the *m*T-AuNP/H-Si LS films (where m = 2 and 4 for Π = 2 and 14 mN m^{-1}), at different stages (or times), are shown in Fig. 6. It is clear from Fig. 6 that a minimum of two Gaussian peaks (one intense and another weak) are necessary to simulate each single peak of the analysed EDPs at the initial stages. The weak peaks are at closer positions to the substrate compared to the corresponding intense peaks, which are at normal positions. Considering these, the coverage (C_L) of the different layers are estimated from the ρ_i value after normalizing with ρ_{max} = 1.6 e Å^{-3} (corresponding to a 100% coverage) and are tabulated (with a closer position first and the normal position second) in Table 2 for the four films at three different stages of time. The coverage (C_S) of different layered (thickness) structures, considering summation of the coverage

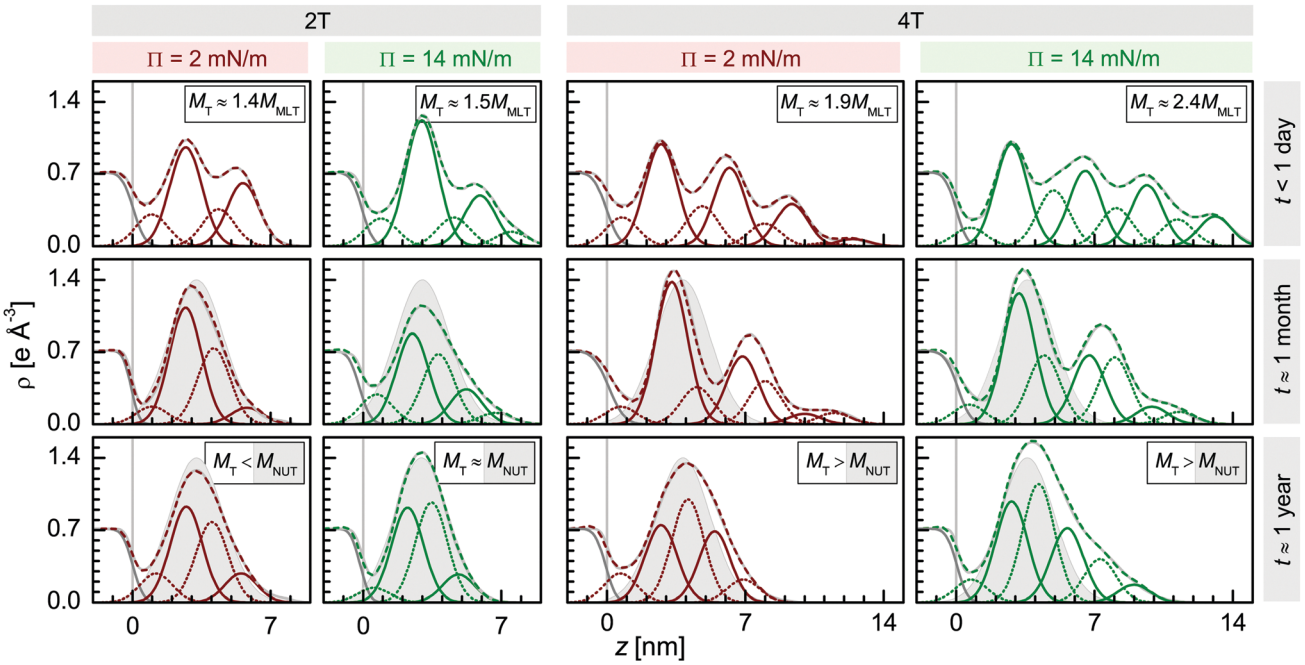

Fig. 6 Gaussian deconvoluted EDPs at different stages (t) of the multi-transferred (2T- and 4T-) AuNP/H-Si LS films prepared from the Langmuir monolayers of two different surface pressures (Π). The EDPs obtained from the XR data analysis are solid gray lines, while the EDPs used for the deconvolution are dashed lines. Each single peak of the EDPs at the initial stages is represented by two Gaussian peaks (of the same width); one at a closer position (dotted lines) and another at the normal position (solid lines) w.r.t. the substrate. Accordingly, all the EDPs are represented by a different series of these alternate peaks. The total amount of transferred material (M_T) w.r.t. the complete monolayer thickness covered material (M_{MLT}) and relative to the complete near unique thickness covered materials ($M_{NUT} \approx 1.5M_{MLT}$, *i.e.* grey filled area) are indicated.

Table 2 The coverage (C_L) of the first (1st), second (2nd), third (3rd) and fourth (4th) layers; and the coverage (C_S) of the monolayer (ML), bilayer (BL), trilayer (TL) and tetralayer (TtL) thickness structures at different stages of time (t). Transferred materials (M_T) w.r.t. complete monolayer thickness covered materials (M_{MLT}) and complete near unique thickness covered materials (M_{NUT}) in the multi-transferred, *m*T-AuNP/H-Si LS films deposited at different surface pressures (Π), as obtained from the deconvolution of the analysed EDPs. Note that each C_L consists of two values (the first one is for the closer position and second one is for the normal position w.r.t. the substrate), while each C_S is the total coverage of similar layered (thickness) structures

			C_L [%]								C_S [%]				M_T	
*m*T	Π [mN m^{-1}]	t	1st		2nd		3rd		4th		TtL	TL	BL	ML	[M_{MLT}]	[M_{NUT}]
2T	2	1 day	19	60	23	38							57	26	~1.4	~0.9
		1 month	11	70	46	11							22	94		
		1 year	17	58	50	17							34	74		
	14	1 day	17	76	17	31	9	0				9	39	45	~1.5	~1.0
		1 month	18	55	43	21	7	0				7	32	59		
		1 year	9	58	60	17							26	92		
4T	2	1 day	17	63	24	47	14	25	2	5	7	32	25	23	~1.9	~1.3
		1 month	10	86	22	42	26	7	7	0	7	11	45	49		
		1 year	17	47	63	43	14	0				14	46	50		
	14	1 day	11	62	34	46	23	37	16	18	29	24	16	27	~2.4	~1.6
		1 month	12	80	42	42	40	11	7	0	7	16	59	40		
		1 year	14	61	72	45	26	11				25	46	62		

of similar layered (thickness) structures even at slightly different positions, are listed in Table 2. Finally, the amounts of transferred material (M_T), as estimated from the C_L or C_S values, are also listed in Table 2.

The values of M_T w.r.t. the full coverage of monolayer thickness (M_{MLT}) indicate that, on average, ~70% and ~74% materials (w.r.t. the monolayer coverage) are transferred each time onto the 2T-AuNP/H-Si LS films deposited at Π = 2 and 14 mN m^{-1}, respectively, while ~48% and ~60% onto the 4T-AuNP/H-Si LS films. Such a decrease in the transfer ratio with an increase of the transfer number, although creating hindrance in the formation of the desired layered structures, is quite natural. An increase of the surface pressure is one way in which one can increase the transfer ratio, to some extent. This is apparent for the 4T-AuNP/H-Si LS films, where about 30% tetralayer is observed for the high pressure (Π = 14 mN m^{-1}) film as opposed to the less than 10% tetralayer for the low pressure (Π = 2 mN m^{-1}) film. Similarly, by tuning the other deposition conditions, it is possible to further improve the transfer ratio to better attain the desired layered structures.

The ambient conditions, on the other hand, play an interesting role on the evolution of the structures of the LS films. The multilayered structures tend toward extended monolayer structures with time; namely for the 2T-AuNP/H-Si LS film deposited at Π = 2 mN m^{-1}, the bilayer structure decreases (~30%) and the monolayer structure increases (~40%). It is found that the final thickness attained by a film depends more on the amount of material transferred (M_T) than on the number of layers. The film with $M_T \approx 1.5M_{MLT}$, attaining a thickness of about 6 nm, is termed as near unique thickness (NUT) with near full coverage, while the films with $M_T < 1.5M_{MLT}$ also attain the NUT but without full coverage. On the other hand, the films with $M_T > 1.5M_{MLT}$ try to attain the NUT but are unable to, as an excess amount can not be accommodated within the NUT. Accordingly, the tetralayer structure in the 4T-AuNP/H-Si LS film deposited at Π = 14 mN m^{-1} decreases (~30%), and in fact vanishes, while both the bilayer and monolayer structures increase (~30%). It can be noted that the film of NUT can accommodate about 1.5 times the amount of material compared to that of the film of MLT, *i.e.* $M_{NUT} \approx 1.5M_{MLT}$. Considering this, the values of M_T are expressed in terms of M_{NUT} in Table 2 for the different films.

3.6 Evolution towards a near unique thickness

The structures of the *m*T-AuNP/H-Si LS films at a particular stage are modeled considering the values of C_L for different vertically positioned layers at that stage, which are shown schematically in Fig. 7. The structures of the films at the initial stages and their evolution with time can be visualized as follows. On the water surface, AuNPs experience both long range vdW attractions and short range steric repulsion, after solvent-evaporation.[6,7,21] This complex interaction leads to the formation of self-assembled disk-like islands of a monolayer height around different points, which on further compression form a

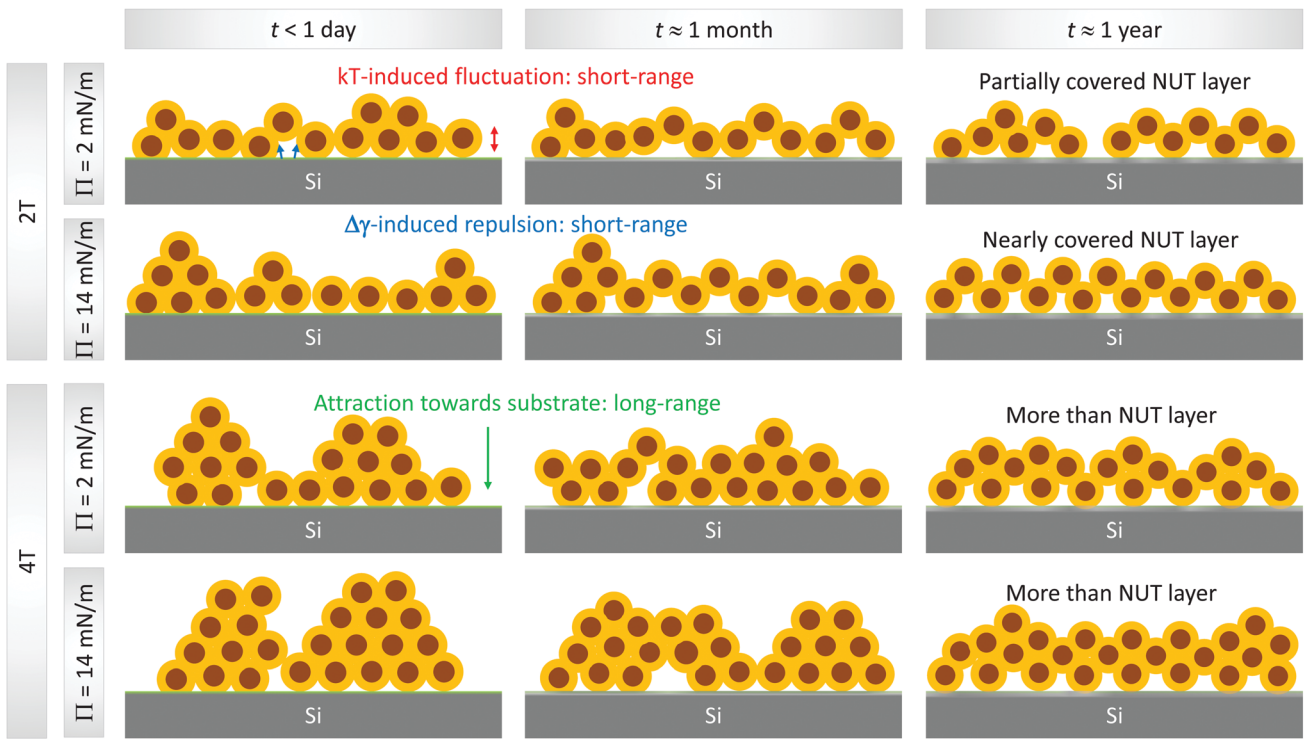

Fig. 7 Structural schematics of multi-transferred (2T- and 4T-) AuNP/H-Si LS films prepared from the Langmuir monolayers of different surface pressures (Π = 2 and 14 mN m^{-1}) at initial stages (t < 1 day), after one month ($t \approx$ 1 month) and after one year ($t \approx$ 1 year) indicating the different processes (namely *kT*-induced effective short-range fluctuation, $\Delta\gamma$-induced short-range repulsion and hydrophobic–hydrophobic interaction mediated effective long-range attraction towards the substrate) involved for the evolution.

thermodynamically stable 2D-network of buckled or flipped disk-like islands.[22,24,44]

During the LS deposition, the hydrophobic terminated Langmuir monolayer feels repulsion from the hydrophilic water and attraction towards the hydrophobic (H-Si or AuNP covered H-Si) substrate, and accordingly layer-by-layer (bi-layer and tetra-layer) growth takes place (as shown schematically in Fig. 7 for $t < 1$ day). However, the multilayers formed on the hydrophobic H-Si substrates become thermodynamically unstable. It is well known that keeping any transferred film for a long time may cause some structural changes (toward the energy minimum state) as the transfer process itself is not always carried out under equilibrium conditions. However, finding the energy minimum state or structure and understanding the actual processes involved in the evolution are very important.

The instability here mainly arises due to the presence of room-temperature thermal energy, kT (where k is the Boltzmann constant and T is the room temperature),[24,27] due to the degradation of thiols at ambient conditions and also due to the change in the substrate surface energy, $\Delta\gamma$ (as some portion of the hydrophobic H-Si surface turns into a weak-hydrophilic O-Si surface through H desorption and O adsorption with time),[24,33] which induces diffusion in the AuNPs. Although thiol oxidation cannot be ruled out under ambient conditions,[45] it is likely that the oxidation is not completely removing the capping layer of the AuNPs. Otherwise continuous growth, due to coalescence of AuNPs with time, would have taken place, which is not the case here (or is at least not the dominating effect). Greater coverage of thiols in curved AuNPs (through defective sites) compared to the planar surfaces[46] probably play an important role in reducing the oxidation of thiols and maintaining some capping on the AuNPs. The certain degradation of thiols (if any) is thus considered here to add extra instability in the system and extra diffusion in the AuNPs, and not to the coalescence of AuNPs.

Each AuNP in the film then experiences hydrophobic–hydrophobic attractive interactions with other AuNPs and/or the H-Si substrate. The AuNPs on the top, where no AuNPs are present above them, experience a net attractive force towards the substrate. These AuNPs, depending upon the availability of the nearest void space, start to roll down or move towards the substrate, to reduce the film thickness (from tetralayers and bilayers toward monolayers) and to increase the film coverage (as shown schematically in Fig. 7 for $t \approx 1$ month and 1 year). However, the $\Delta\gamma$-energy in some portion of the substrate surface creates repulsion and the kT-energy creates fluctuation on the AuNPs, which altogether imposes restriction in the thickness reduction and ideal monolayer formation, and rather deviates to form a thermodynamically favourable and relatively stable extended monolayer of NUT. It is necessary to mention that, through reorganization, such a NUT layer can be formed if the number (N) of AuNPs in the multilayer is less than (as shown in Fig. 7 for the the 2T and $\Pi = 2$ mN m^{-1} film) or equal to (as shown in Fig. 7 for the 2T and $\Pi = 14$ mN m^{-1} film) the maximum number (N_c) of AuNPs that can be accommodated within the NUT. Otherwise (if $N > N_c$), the evolved-thickness will increase (as shown in Fig. 7 for the 4T films) to accommodate extra particles. The reorganization process (*i.e.* the duration of reorganization) depends on the number of voids and AuNPs. Accordingly, the reorganization or the thickness-decrease process continues for a longer time ($t > 1$ month) for the films with a larger number of partial coverage layers (as shown in Fig. 7 for the 4T films).

It can be noted that the mechanistic origins for lamellar instability and the convergent reorganization of multilayers proposed here strongly depend on the roles of the thermal fluctuations, the hydrophobic repulsion between nanoparticles and the degradation of thiols. Hence they call for additional experiments to firmly validate the proposed mechanism. Specifically, it is important to examine how temperature, surface hydrophobicity (which can be controlled by mixing hydrophilic and hydrophobic thiols), and the size of the nanoparticles affect the stability and the NUT. Also, the assumption that the degradation of thiols only adds extra diffusion in the AuNPs and not to the coalescence, seems to be valid but deserves direct experimental verification.

4 Conclusions

The structural evolution of multi-transferred LS films of AuNPs on H-passivated Si substrates has been investigated using XR and GISAXS techniques. It is found from this structural investigation that the number of layers transferred onto the substrate is proportional to the number of transfers, but the coverage of the layer decreases considerably with the increase in the number of layers. Such fractional coverage multilayered structures are quite unstable at ambient conditions. The instability mainly arises from three factors: (i) the room-temperature thermal energy (kT) induced fluctuation, (ii) the change in the substrate surface energy ($\Delta\gamma$) induced repulsion and (iii) the dissimilar film–substrate and film–air interfacial interaction induced attractions towards the substrate. Such instability, in one hand, creates hindrance in the control and formation of desired 3D-nanostructures through a bottom-up approach. On the other hand, the same instability decreases the film thickness and tries to form a near unique thickness (NUT) through the reorganization of AuNPs for a different duration. The duration of reorganization increases with the increase of layer number. The value of NUT ($\sim$6 nm) is greater than the thickness of the ideal monolayer ($\sim$4.5 nm) but less than the thickness of the ideal bilayer ($\sim$9 nm). This value of NUT is actually related to the size of the AuNPs ($\sim$4.5 nm) plus their possible fluctuation ($\sim$1.5 nm) due to the kT-energy. The formation of the NUT layer (for $N \leq N_c$), through reorganization, is quite distinctive. In fact, the NUT layer is found to evolve through three complex processes and interactions, namely (i) the decrease of thickness (or roll down of the top AuNPs through the nearest void space) due to the anisotropic hydrophobic–hydrophobic interaction mediated long range attractions towards the substrate, (ii) the increase of thickness due to the anisotropic hydrophilic–hydrophobic interaction mediated short range repulsion from the substrate, and (iii) the increase in

thickness due to the *kT*-energy induced effective outward fluctuation w.r.t. the substrate. However, further experiments are needed to firmly validate the proposed mechanism.

Conflicts of interest

There are no conflicts to declare.

Acknowledgements

The authors thank Dr S. V. Roth for his support in the GISAXS measurements. The financial support received from the Saha Institute of Nuclear Physics under the DST-DESY project to carry out GISAXS experiments at PETRA III is thankfully acknowledged.

References

1 M. C. Daniel and D. Astruc, *Chem. Rev.*, 2004, **104**, 293–346.
2 *Clusters and Colloids: From Theory to Applications*, ed. G. Schmid, John Wiley & Sons, 2008.
3 Y. Yu, A. Jain, A. Guillaussier, V. R. Voggu, T. M. Truskett, D.-M. Smilgies and B. A. Korgel, *Faraday Discuss.*, 2015, **181**, 181–192.
4 G. F. Mancini, T. Latychevskaia, F. Pennacchio, J. Reguera, F. Stellacci and F. Carbone, *Nano Lett.*, 2016, **16**, 2705–2713.
5 C. B. Murray, C. R. Kagan and M. G. Bawendi, *Annu. Rev. Mater. Sci.*, 2000, **30**, 545–610.
6 E. Rabani, D. R. Reichman, P. L. Geissler and L. E. Brus, *Nature*, 2003, **426**, 271–274.
7 T. P. Bigioni, X.-M. Lin, T. T. Nguyen, E. I. Corwin, T. A. Witten and H. M. Jaeger, *Nat. Mater.*, 2006, **5**, 265–270.
8 Y. Min, M. Akbulut, K. Kristiansen, Y. Golan and J. Israelachvili, *Nat. Mater.*, 2008, **7**, 527–538.
9 Z. Nie, A. Petukhova and E. Kumacheva, *Nat. Nanotechnol.*, 2010, **5**, 15–25.
10 J. F. Galisteo-López, M. Ibisate, R. Sapienza, L. S. Froufe-Pérez, A. Blanco and C. López, *Adv. Mater.*, 2011, **23**, 30–69.
11 B. T. Diroll, K. M. Weigandt, D. Jishkariani, M. Cargnello, R. J. Murphy, L. A. Hough, C. B. Murray and B. Donnio, *Nano Lett.*, 2015, **15**, 8008–8012.
12 J. Yang, M. K. Choi, D.-H. Kim and T. Hyeon, *Adv. Mater.*, 2016, **28**, 1176–1207.
13 J. Y. Kim, S. J. Kwon, J.-B. Chang, C. A. Ross, T. A. Hatton and F. Stellacci, *Nano Lett.*, 2016, **16**, 1352–1358.
14 M. A. Boles, M. Engel and D. V. Talapin, *Chem. Rev.*, 2016, **116**, 11220–11289.
15 M. Brust, M. Walker, D. Bethell, D. J. Schiffrin and R. Whyman, *J. Chem. Soc., Chem. Commun.*, 1994, 801–802.
16 S. Liu, R. Maoz and J. Sagiv, *Nano Lett.*, 2004, **4**, 845–851.
17 D. G. Schultz, X.-M. Lin, D. Li, J. Gebhardt, M. Meron, P. J. Viccaro and B. Lin, *J. Phys. Chem. B*, 2006, **110**, 24522–24529.
18 M. K. Bera, M. K. Sanyal, S. Pal, J. Daillant, A. Datta, G. U. Kulkarni, D. Luzet and O. Konovalov, *Europhys. Lett.*, 2007, **78**, 56003.
19 R. Banerjee, S. Hazra, S. Banerjee and M. K. Sanyal, *Phys. Rev. E: Stat., Nonlinear, Soft Matter Phys.*, 2009, **80**, 056204.
20 M. A. Mezour, I. I. Perepichka, J. Zhu, R. B. Lennox and D. F. Perepichka, *ACS Nano*, 2014, **8**, 2214–2222.
21 K. Z. Milowska and J. K. Stolarczyk, *Phys. Chem. Chem. Phys.*, 2016, **18**, 12716–12724.
22 M. Mukhopadhyay and S. Hazra, *RSC Adv.*, 2016, **6**, 12326–12336.
23 I. Kosif, K. Kratz, S. S. You, M. K. Bera, K. Kim, B. Leahy, T. Emrick, K. Yee, C. Lee and B. Lin, *ACS Nano*, 2017, **11**, 1292–1300.
24 M. Mukhopadhyay and S. Hazra, *Phys. Chem. Chem. Phys.*, 2018, **20**, 1051–1062.
25 I. K. Robinson and D. J. Tweet, *Rep. Prog. Phys.*, 1992, **55**, 599–651.
26 *X-Ray and Neutron Reflectivity: Principles and Applications*, ed. J. Daillant and A. Gibaud, Springer, Paris, 1999.
27 J. K. Bal and S. Hazra, *Phys. Rev. B: Condens. Matter Mater. Phys.*, 2007, **75**, 205411.
28 J. K. Bal and S. Hazra, *Phys. Rev. B: Condens. Matter Mater. Phys.*, 2009, **79**, 155405.
29 I. Roy and S. Hazra, *Soft Matter*, 2015, **11**, 3724–3732.
30 S. Hazra, A. Gibaud, A. Désert, C. Sella and A. Naudon, *Physica B*, 2000, **283**, 97–102.
31 P. Chatterjee, S. Hazra and H. Amenitsch, *Soft Matter*, 2012, **8**, 2956–2964.
32 J. K. Bal and S. Hazra, *Phys. Rev. B: Condens. Matter Mater. Phys.*, 2009, **79**, 155412.
33 J. K. Bal, S. Kundu and S. Hazra, *Phys. Rev. B: Condens. Matter Mater. Phys.*, 2010, **81**, 045404.
34 D. V. Leff, P. C. Ohara, J. R. Heath and W. M. Gelbart, *J. Phys. Chem.*, 1995, **99**, 7036–7041.
35 H. F. Okorn-Schmidt, *IBM J. Res. Dev.*, 1999, **43**, 351–366.
36 I. Langmuir and V. J. Schaefer, *J. Am. Chem. Soc.*, 1938, **60**, 1351.
37 S. Hazra, *Appl. Surf. Sci.*, 2006, **253**, 2154–2157.
38 S. V. Roth, G. Herzog, V. Körstgens, A. Buffet, M. Schwartzkopf, J. Perlich, M. M. A. Kashem, R. Döhrmann, R. Gehrke, A. Rothkirch, K. Stassig, W. Wurth, G. Benecke, C. Li, P. Fratzl, M. Rawolle and P. Müller-Buschbaum, *J. Phys.: Condens. Matter*, 2011, **23**, 254208.
39 A. Buffet, A. Rothkirch, R. Döhrmann, V. Körstgens, M. M. A. Kashem, J. Perlich, G. Herzog, M. Schwartzkopf, R. Gehrke, P. Müller-Buschbaum and S. V. Roth, *J. Synchrotron Radiat.*, 2012, **19**, 647–653.
40 P. Chatterjee and S. Hazra, *Soft Matter*, 2013, **9**, 9799–9806.
41 P. Chatterjee and S. Hazra, *J. Phys. Chem. C*, 2014, **118**, 11350–11356.
42 I. Roy and S. Hazra, *RSC Adv.*, 2015, **5**, 665–675.
43 L. G. Parratt, *Phys. Rev.*, 1954, **95**, 359–369.
44 A. Huerre, F. Cacho-Nerin, V. Poulichet, C. E. Udoh, M. D. Corato and V. Garbin, *Langmuir*, 2018, **34**, 1020–1028.
45 T. M. Willey, A. L. Vance, T. van Buuren, C. Bostedt, L. J. Terminello and C. S. Fadley, *Surf. Sci.*, 2005, **576**, 188–196.
46 C. Vericat, M. E. Vela, G. Benitez, P. Carrob and R. C. Salvarezza, *Chem. Soc. Rev.*, 2010, **39**, 1805–1834.

